Обзор ArXiv: astro-ph, 1-5 апреля 2019 года

От Сильченко О.К.

ArXiv: 1904.00695

Extended star-forming region within galaxies in a dense proto-cluster core at z=2.53*

Tomoko L. Suzuki[1,2], Yosuke Minowa[3,4], Yusei Koyama[3,4], Tadayuki Kodama[1], Masao Hayashi[2], Rhythm Shimakawa[3], Ichi Tanaka[3], Ken-ichi Tadaki[2]

[1]Astronomical Institute, Tohoku University, 6-3 Aramaki, Aoba-ku, Sendai, Miyagi 980-8578, Japan
[2]National Astronomical Observatory of Japan, 2-21-1 Osawa, Mitaka, Tokyo 181-8588, Japan
[3]Subaru Telescope, National Astronomical Observatory of Japan, National Institutes of Natural Sciences, 650 North A'ohoku Place, Hilo, HI 96720, USA
[4]Department of Astronomical Science, SOKENDAI (The Graduate University for Advanced Studies), 2-21-1 Osawa, Mitaka, Tokyo 181-8588, Japan

*E-mail: suzuki.tomoko@astr.tohoku.ac.jp

Received ⟨reception date⟩; Accepted ⟨acception date⟩

Выборка галактик с эмиссией в скоплении на z=2.53

Object InfraRed Camera and Spectrograph (MOIRCS; Ichikawa et al. 2006). So far, 107 Hα emitters are identified in this proto-cluster based on color-color selections (Hayashi et al. 2012, 2016; Shimakawa et al. 2018).

The spatial distribution of the Hα emitters in USS1558 is characterized by several groups of Hα emitters. The densest group is located at 1.5 Mpc away from the radio galaxy (figure 5 in Hayashi et al. (2012)), and its local surface density is 30 times higher than that in the general field (Hayashi et al. 2012). We observed this densest group with Subaru/IRCS+AO188. In total, 20 Hα emitters are covered in the IRCS FoV (53×53 arcsec^2).

Финальная выборка и наблюдения

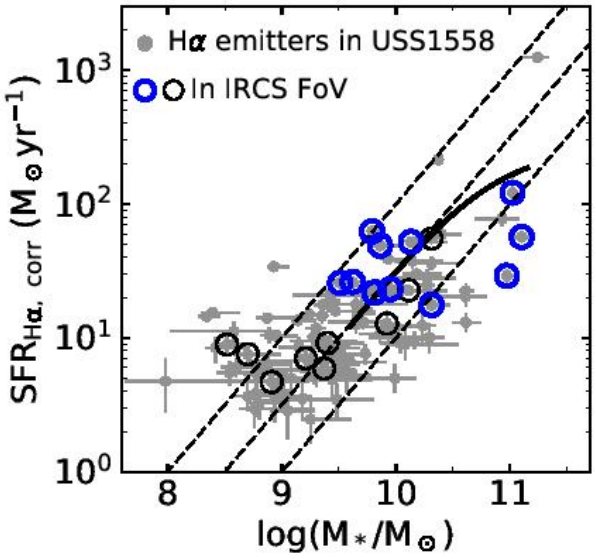

Fig. 1. Stellar mass–SFR relation for the Hα emitters in USS1558 (Hayashi et al. 2012, 2016; Shimakawa et al. 2018). Open circles show the Hα emitters covered in the IRCS FoV. The blue thick ones correspond to the Hα emitters analyzed in this study (subsection 2.2). Dotted lines represent constant sSFRs ($\mathrm{SFR}/\mathrm{M}_*$), namely, $\log(\mathrm{sSFR}\ [\mathrm{yr}^{-1}]) = -8.0, -8.5, \mathrm{and} -9.0$. The thick solid line shows the star-forming main sequence at $z = 2.53$ from Tomczak et al. (2016). Our IRCS+AO188 targets are located around the "main sequence" of star-forming galaxies at this epoch.

Table 1. Summary of the obtained data in USS1558 with IRCS+AO188. The limiting magnitude is obtained with a 0.5 arcsec diameter aperture.

Band	Dates (UT)	Exposure time (hours)	FWHM (arcsec)	$m_{\mathrm{lim},3\sigma}$ (mag)	AO mode
K'	2013 May 7	2.2	0.25	25.55	LGS
NB2315	2014 May 17, 18, 22	7.4	0.17	24.09	LGS

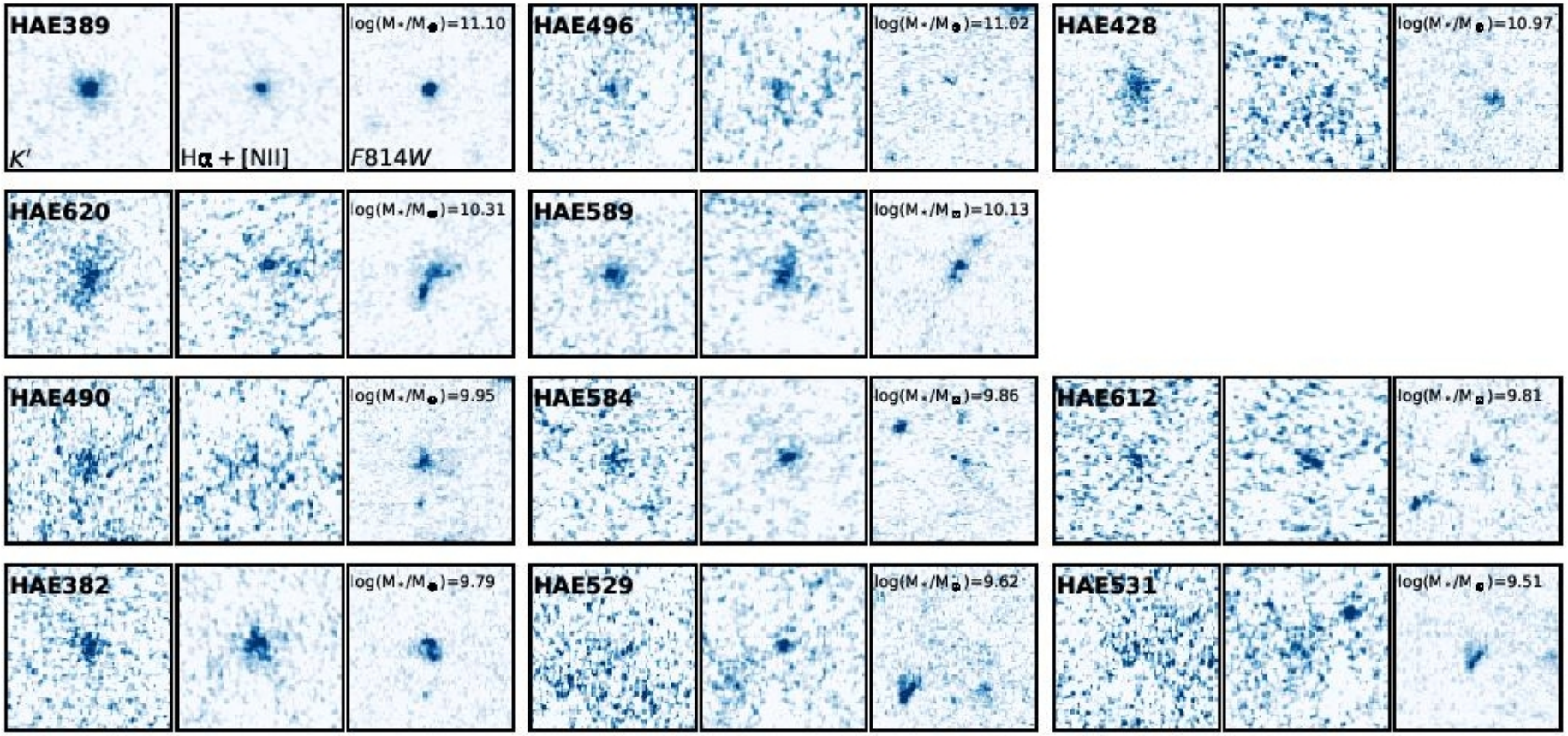

Fig. 2. The IRCS/K', IRCS/NB2315$-K'$, and ACS/I_{F814W} images for 11 Hα emitters in the densest group in USS1558 (the image size is $4.3 \times 4.3\,\mathrm{arcsec}^2$). The K' and NB2315$-K'$ images correspond to the stellar continuum and Hα+[NII] emission line, respectively. The I_{F814W} images correspond to the rest-frame 2300 Å at $z \sim 2.53$. The IRCS+AO188 images have a similar resolution as HST. The top two rows show the Hα emitters with $10.0 \leq \log(\mathrm{M}_*/\mathrm{M}_\odot) \leq 11.1$ (high-mass sub-sample). The bottom two rows show the Hα emitters with $9.5 \leq \log(\mathrm{M}_*/\mathrm{M}_\odot) < 10.0$ (low-mass sub-sample). IDs are extracted from the catalog by Hayashi et al. (2016), and stellar masses are estimated by Shimakawa et al. (2018).

Изображения, сложенные в бинах по массам

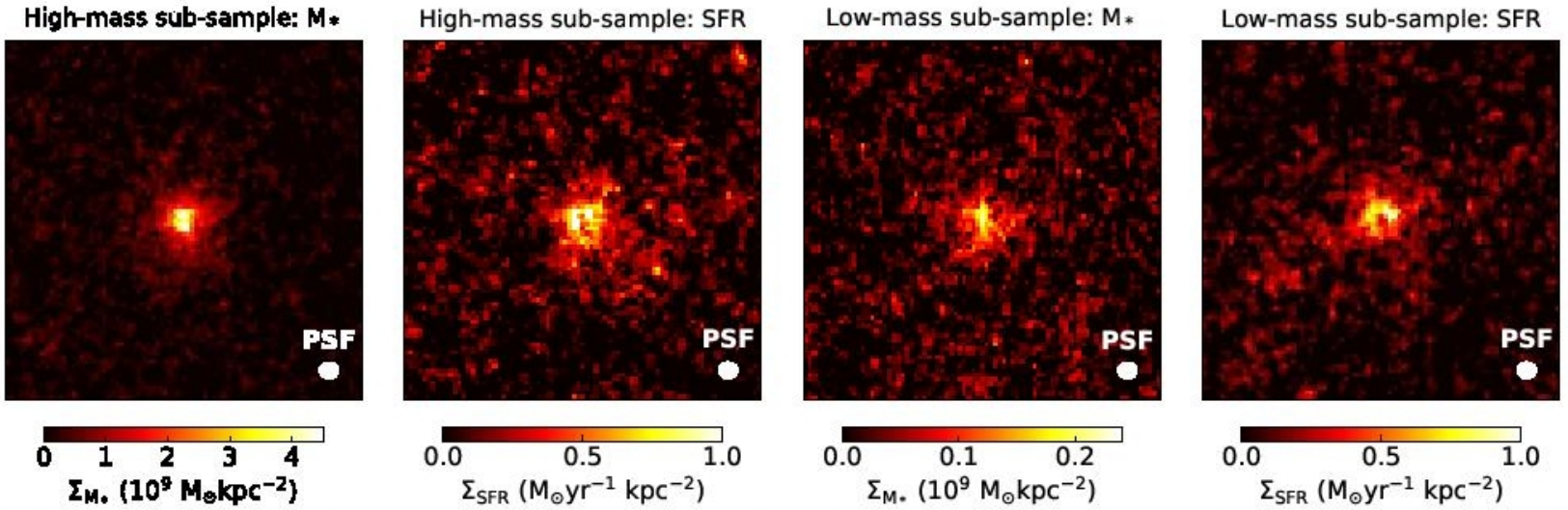

Fig. 4. Stacked images of the stellar mass and $\mathrm{SFR}_{\mathrm{H}\alpha,\mathrm{corr}}$ for the two sub-samples with the radially dependent $\mathrm{A}_{\mathrm{H}\alpha}$ (subsection 4.1). The box size of each panel is $\sim 4.3 \times 4.3\,\mathrm{arcsec}^2$. The small white circle in each panel shows the PSF size (FWHM).

Размеры в континууме и в линии

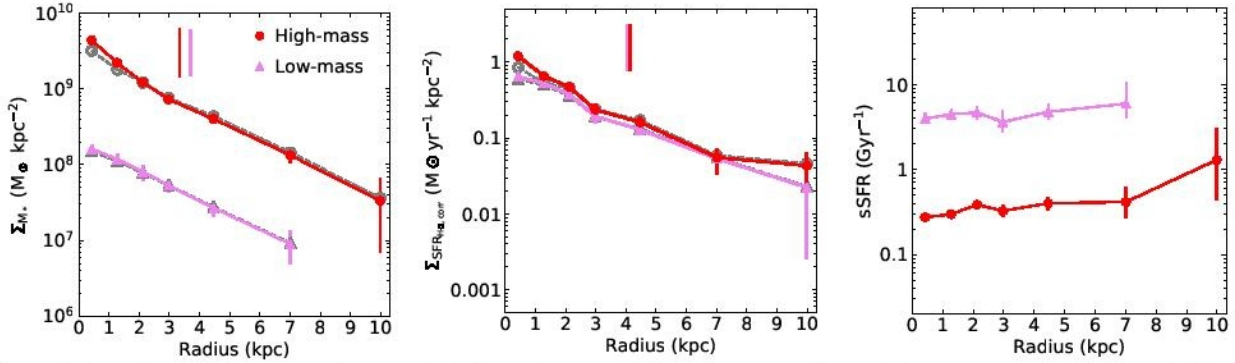

Fig. 5. Radial profiles of the two sub-samples. From the left to right, each panel shows the radial profiles of stellar mass surface density, those of SFR surface density, and those of sSFR. In the left and the middle panels, the filled symbols represent the results using the radially dependent $A_{H\alpha}$ (subsection 4.1). The open symbols represent the results with the uniform $A_{H\alpha}$. The vertical lines in the left and middle panel represent $R_{1/2}$ for the stellar component and star-forming region with the radially dependent $A_{H\alpha}$. The thick ones show $R_{1/2}$ for the high-mass sub-sample. The SFR profiles of the two sub-samples have a flatter slope than the stellar mass profiles.

Table 2. Summary of the total stellar mass, dust-extinction-corrected total SFRs, and sizes of the stellar components and star-forming regions for the two sub-samples in USS1558.

	Total		Radially dependent $A_{H\alpha}$		Uniform $A_{H\alpha}$	
	Stellar mass $\log(M_*/M_\odot)$	$SFR_{H\alpha,corr}$ $(M_\odot yr^{-1})$	$R_{1/2}(M_*)$ (kpc)	$R_{1/2}(SFR_{H\alpha,corr})$ (kpc)	$R_{1/2}(M_*)$ (kpc)	$R_{1/2}(SFR_{H\alpha,corr})$ (kpc)
High-mass	10.97	37.77	$3.34^{+0.16}_{-0.15}$	4.13 ± 0.11	3.65 ± 0.16	4.37 ± 0.13
Low-mass	9.80	28.23	$3.70^{+0.45}_{-0.39}$	4.02 ± 0.23	$3.77^{+0.46}_{-0.39}$	$4.12^{+0.24}_{-0.23}$

Сравнение скопления и поля на z=2.5

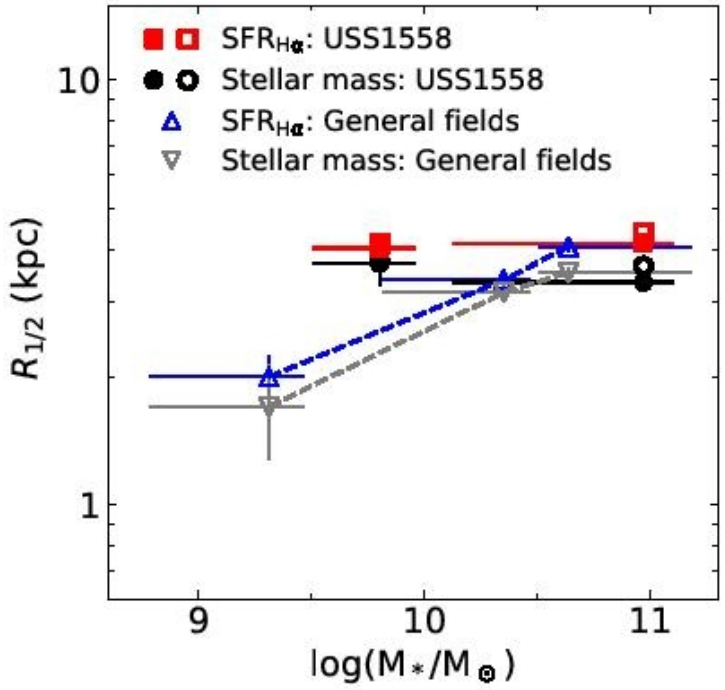

Fig. 6. Relation between the total stellar mass and size of the stellar components and star-forming regions for the Hα emitters in different density fields at $z = 2 - 2.5$. The sizes measured in the stacked images are shown for the two samples. The filled symbols represent $R_{1/2}$ assuming the radially dependent $\mathrm{A_{H\alpha}}$, whereas the open symbols represent $R_{1/2}$ obtained with the uniform $\mathrm{A_{H\alpha}}$. Both in the general fields and in the proto-cluster core, star-forming regions are more extended than the underlying stellar components at least for the massive star-forming galaxies with $\log(\mathrm{M_*/M_\odot}) \sim 10 - 11$.

ArXiv: 1904.01260

The Fornax 3D project: Thick disks in a cluster environment

F. Pinna[1,2,⋆], J. Falcón-Barroso[1,2], M. Martig[3], L. Coccato[4], E. M. Corsini[5,6], P.T. de Zeeuw[7,8], D.A. Gadotti[4], E. Iodice[9], R. Leaman[10], M. Lyubenova[4], I. Martín-Navarro[11,10] L. Morelli[12,6], M. Sarzi[13], G. van de Ven[14,4], S. Viaene[15,16], R.M. McDermid[17,18]

[1] Instituto de Astrofísica de Canarias, Calle Via Láctea s/n, E-38200 La Laguna, Tenerife, Spain
[2] Depto. Astrofísica, Universidad de La Laguna, Calle Astrofísico Francisco Sánchez s/n, E-38206 La Laguna, Tenerife, Spain
[3] Astrophysics Research Institute, Liverpool John Moores University, 146 Brownlow Hill, Liverpool L3 5RF, UK
[4] European Southern Observatory, Karl-Schwarzschild-Strasse 2, 85748 Garching bei Muenchen, Germany
[5] Dipartimento di Fisica e Astronomia 'G. Galilei', Università di Padova, vicolo dell'Osservatorio 3, I-35122 Padova, Italy
[6] INAF–Osservatorio Astronomico di Padova, vicolo dell'Osservatorio 5, I-35122 Padova, Italy
[7] Sterrewacht Leiden, Leiden University, Postbus 9513, 2300 RA Leiden, The Netherlands
[8] Max-Planck-Institut fuer extraterrestrische Physik, Giessenbachstrasse, 85741 Garching bei Muenchen, Germany
[9] INAF–Osservatorio Astronomico di Capodimonte, via Moiariello 16, I-80131 Napoli, Italy
[10] Max-Planck Institut fuer Astronomie, Konigstuhl 17, D-69117 Heidelberg, Germany
[11] University of California Observatories, 1156 High Street, CA-95064, Santa Cruz, USA
[12] Instituto de Astronomía y Ciencias Planetarias, Universidad de Atacama, Copiapó, Chile
[13] Armagh Observatory and Planetarium, College Hill, Armagh, BT61 9DG, UK
[14] Department of Astrophysics, University of Vienna, Türkenschanzstrasse 17, 1180 Wien, Austria
[15] Sterrenkundig Observatorium, Universiteit Gent, Krijgslaan 281, B-9000 Gent, Belgium
[16] Centre for Astrophysics Research, University of Hertfordshire, College Lane, Hatfield AL10 9AB, UK
[17] Department of Physics and Astronomy, Macquarie University, Sydney, NSW 2109, Australia
[18] Australian Astronomical Observatory, PO Box 915, Sydney, NSW 1670, Australia

Fornax!

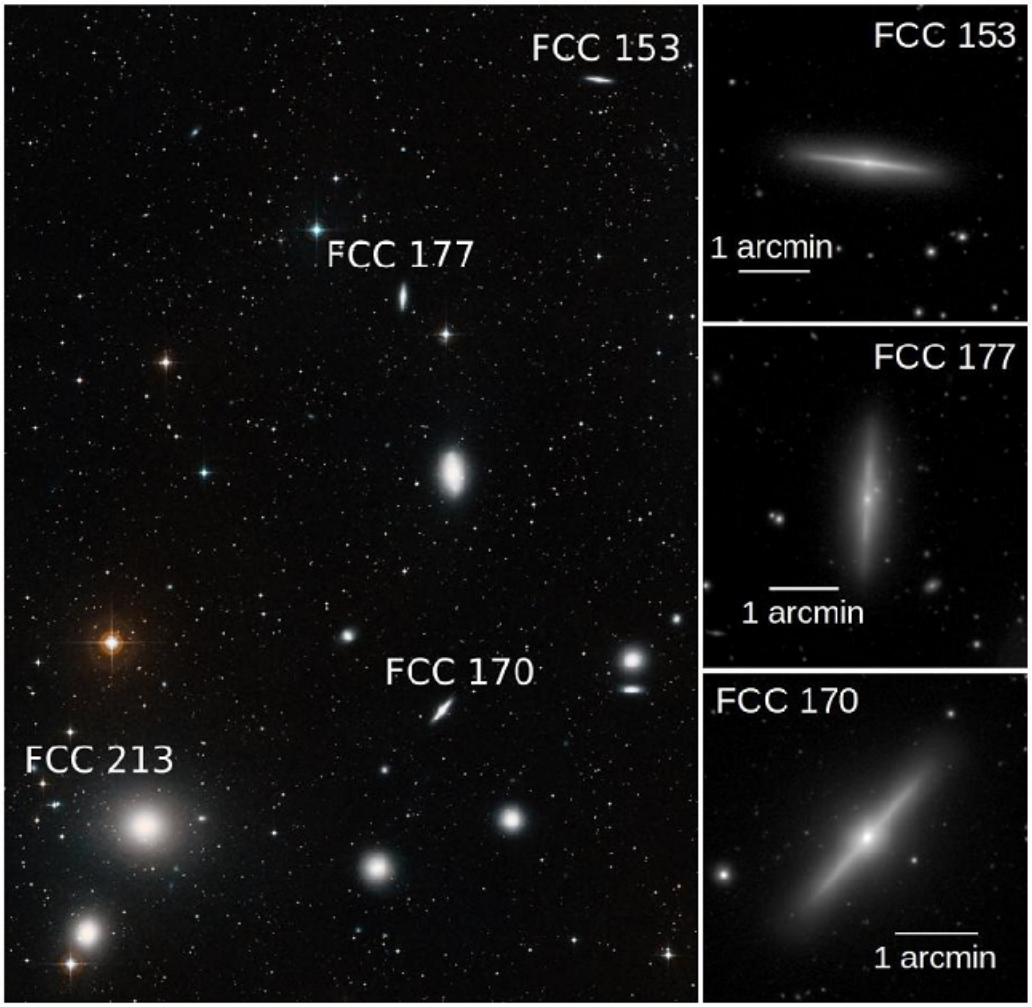

Fig. 1. Left: clipping of the wide-field view of the Fornax Galaxy Cluster (credit: ESO and Digitized Sky Survey 2, acknowledgment: David Martin). The three galaxies analyzed in Paper I and this paper are indicated with their names. FCC 213 is the central galaxy of the cluster. R *r*-band images from the Fornax Deep Survey (Iodice et al. 2019). From top to bottom: FCC 153, FCC 177 and FCC 170. A scale bar is indi in each image.

Результаты для IC 335

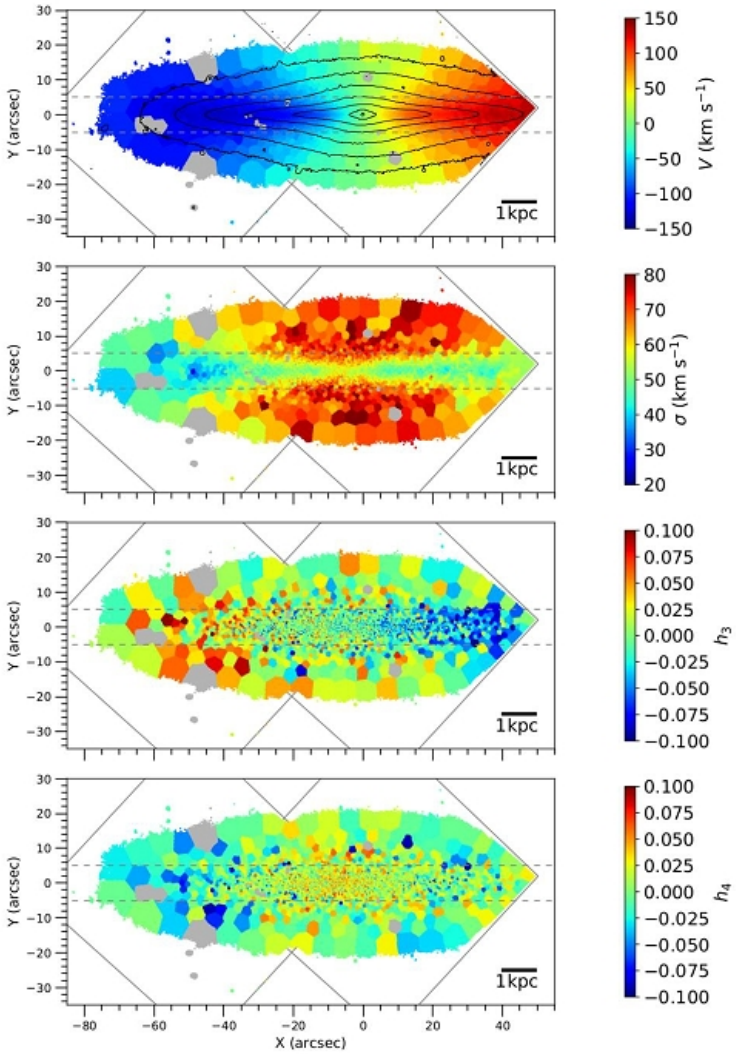

Fig. 2. Maps of the stellar kinematics of FCC 153. From top to bottom: mean velocity V, velocity dispersion σ, skewness h_3 and kurtosis h_4. The discarded bins are plotted in grey, as well as the coverage of the two MUSE pointings. The physical units are indicated by the scale bar on bottom-right of each panel. The horizontal dashed lines indicate $\pm z_{c1}$. In the top panel, contours of surface brightness are plotted in black.

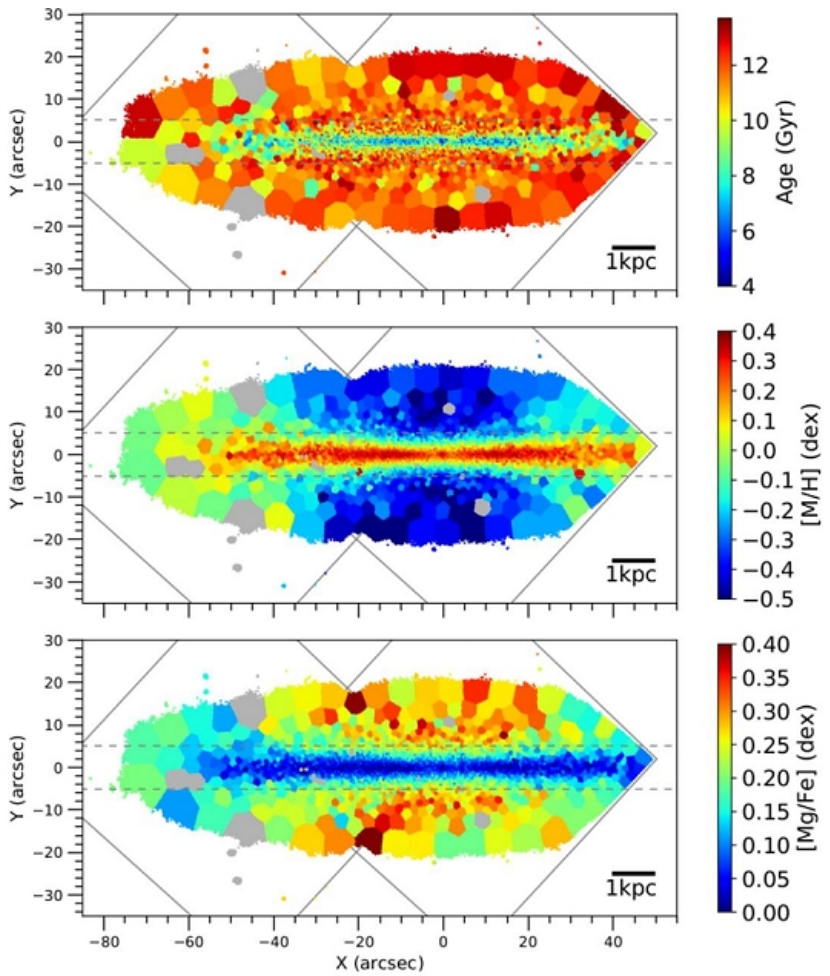

Fig. 4. Stellar-population maps for FCC 153. From top to bottom: mean age, total metallicity [M/H], [Mg/Fe] abundance. The discarded bins are plotted in grey, as well as the coverage of the two MUSE pointings. The physical units are indicated by the scale bar on bottom-right of each panel. The horizontal dashed lines indicate $\pm z_{c1}$.

Результаты для NGC 1380A

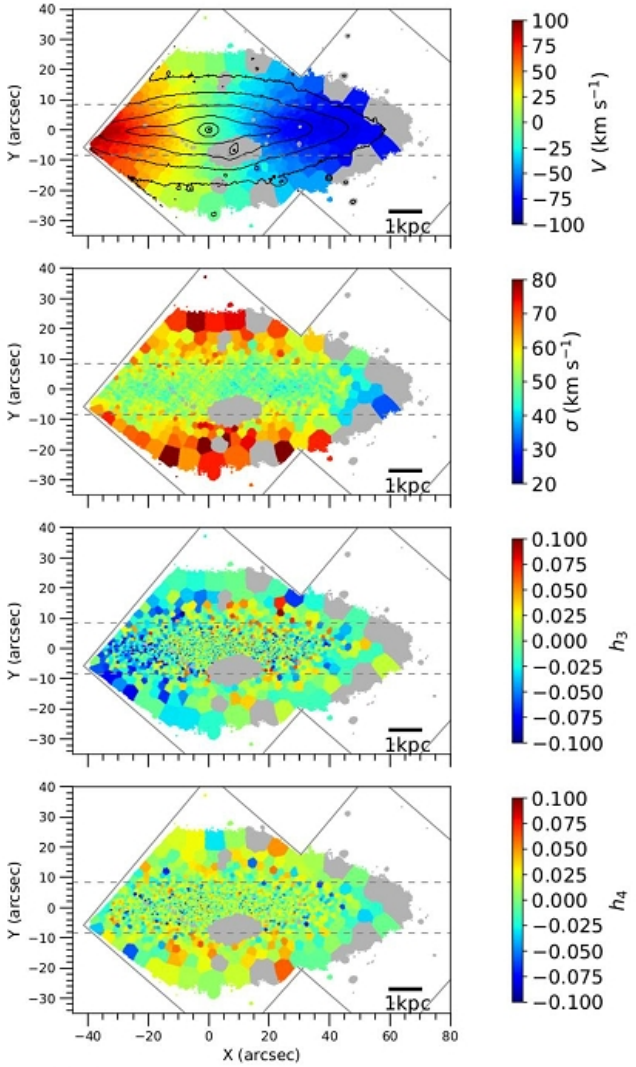

Fig. 3. As Fig. 2, now for FCC 177.

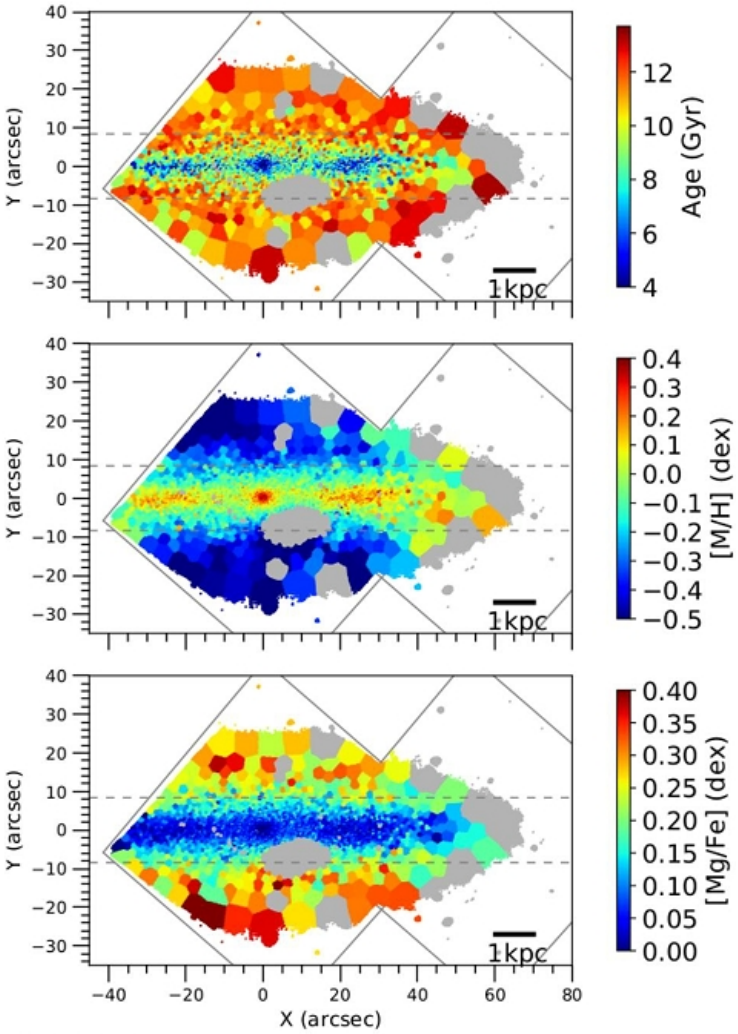

Fig. 5. As Fig. 4, now for FCC 177.

we will refer to its enhancement also as "α-enhancement", often

the maps of the mean stellar-population properties of F

И опять истории звездообразования!

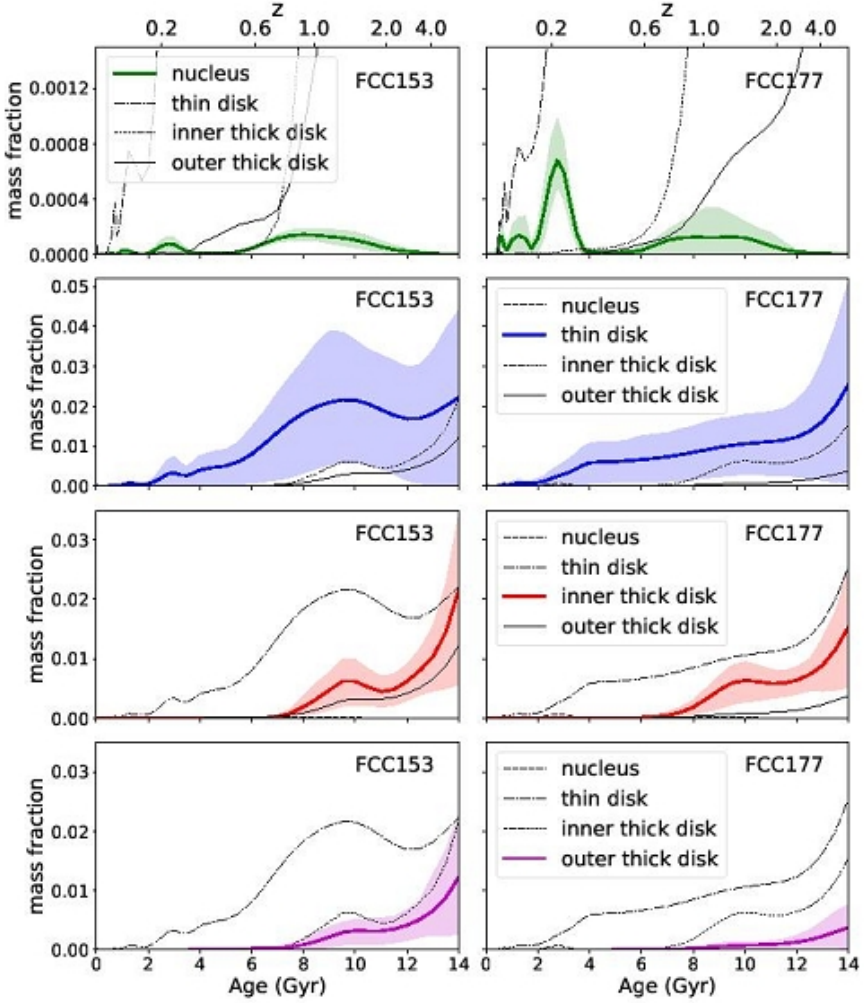

Fig. 8. As in Fig. 7 but now the mass fraction is normalized to the total mass of the galaxy.

Весьма экзотические…

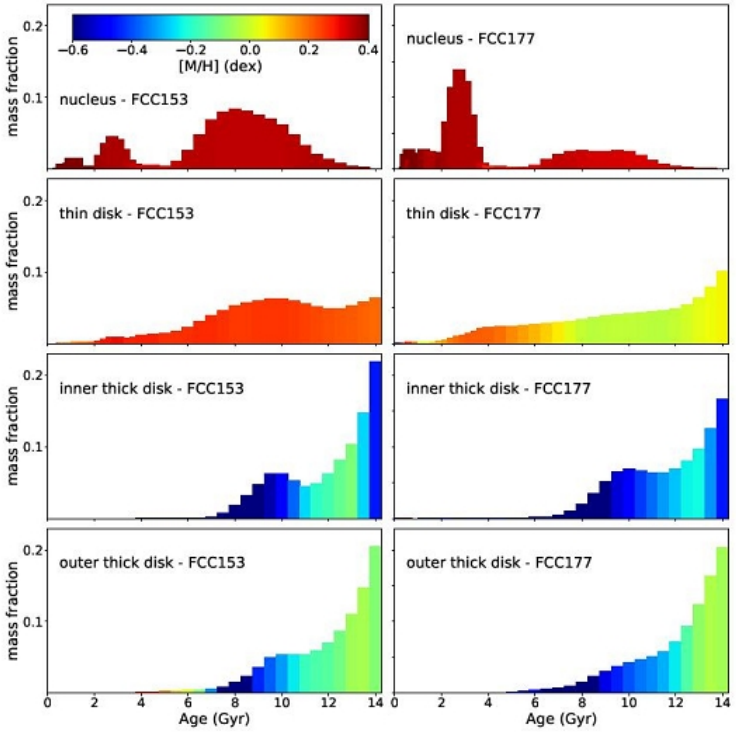

Fig. 9. SFH of the different structural components of FCC 153 (left panels) and FCC 177 (right panels). From top to bottom: disk, the inner and the outer thick disk. The histogram age bins are color coded according to the weighted average total metal specific age bin. The average mass fraction is displayed on the vertical axis, weighted by the mass in each bin and normaliz component.

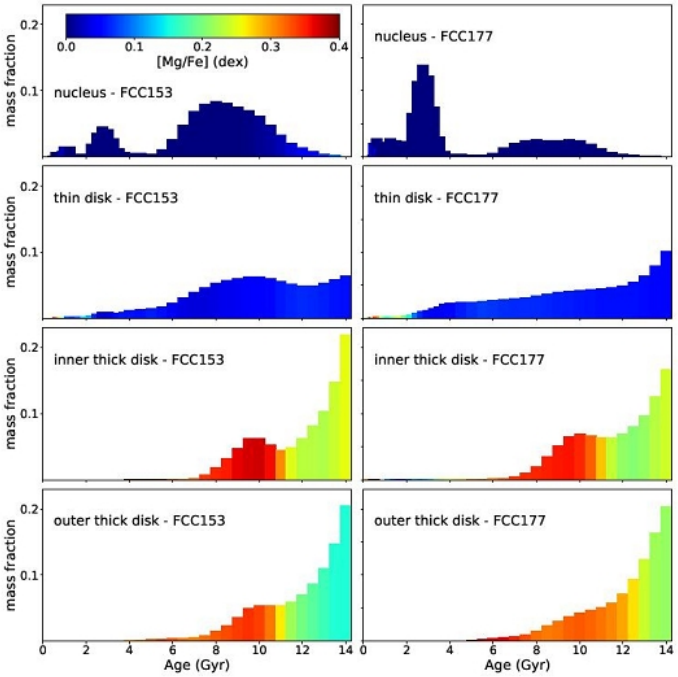

Fig. 10. As in Fig. 9, but now the histogram age bins are color coded according to the weighted average [Mg/Fe] of the specific age bin.